Self-Organized Criticality: On Generalized Sandpile Models

COMP90072: The Art of Scientific Computation

Final Report

Wenrui Yuan

School of Mathematics and Statistics

8th November 2020

Contents

1 Introduction and Overview

Self-Organized Crticality (SOC) is concept that has been studied by many to understand complex phenomena in nature that cannot be measured. In general, criticality is a behavior where a equilibrium system with set of parameters undergoes a phase transition that takes it to a normally disordered phase. First introduced by Bak, Tang and Wiesenfeld in 1987 to explain the $1/f$ noise [1], the concept was first interpreted as a non-equilibrium dynamical system with a critical state attractor that exhibits long range spatial or temporal scale invariance with extended degrees of freedom, whose phase transition is not controlled by predefined methods or parameters, as the system drive it self to criticality. In [1, 2], they studied the cascading effect of small local perturbations on a structure of minimally stable through a simple sandpile model, later proven to be Abelian, that exhibits the power-law behavior. The sandpile model was further investigated through simulation in presenting the temporal and spatial correlations and thus identifies the $1/f$ noise [2], and scale invariance allows the study of other dynamical systems that admit SOC on power-law spectrum [3]. The original model was generalized by Chau and Cheng through establishing the fundamental model, rendering the device for creating sandpile models that obeys critical exponent distribution [4]. Other evolved models, although showing the power-law distributions, whose results often deviate from the original model, demand studies in more generalized context[5, 6]. Critical slope models were studied and believed to be non-Abelian due to non commutative toppling configurations and disagreement in simulation results with general Abelian models [7, 8].

In this report, we will examine the Abelian sandpile model by studying its power-law behavior and spatially scale invariant dynamics. The main goal is to validate results from previous studies by a combination of mathematical proofs and simulation results. We will also study two variants of this model and thus determine which model emulates a more realistic avalanching dynamics.

Structures of this report is as follows: section 2 will cover models and implementation methods, where arguments are mainly focused on the general Abelian sandpile as for its mathematical soundness. Section 3 will be primarily simulation results under different constraints, followed by conclusions and discussion in section 4.

2 Model and Method

2.1 Scale invariance

Before defining the actual model, one should understand correlations between phenomena that follow power-law distribution and scale invariance, which is often defined under a class of functions

$$f(\lambda x) = C(\lambda) f(x),$$

where λ is the scaling factor. One example is monomials, $f(x) = x^n$, which follows

$$f(\lambda x) = (\lambda x)^n = \lambda^n x^n,$$

where λ^n is the scaling exponent with degree n. Hence, the power-law function of the form $f(x) = ax^k$ can be applied to a wide range of dynamical systems that exhibit scale invariance.

2.2 Abelian sandpile model

For a initially empty, finite size surface, if we add a grain of sand randomly per unit time, then sand grains will accumulate until a certain critical state, where grains start to fall off. In reality, one would expect such a behavior does not change even on a sufficient large finite size surface, which is equivalent to scale invariance: if a local perturbation (i.e. a drop of sand) is introduced to the minimally stable system, then the system becomes unstable, triggering more avalanches that can no longer described by the local dynamics. In words, the sandpile is self-governed, and critical state is only determined by the exponent.

Another important aspect of this model is the restriction of finite size; suppose instead that a infinite size surface is given, what is the relaxation time for this system? Or, if the initial empty assumption is given, how long would it take to cause an avalanche? Although studies have ensured convergence with the latter configuration, it is highly subject to initial conditions [9, 10].

2.2.1 Bak-Tang-Wiesenfeld model

The original model in 2D was defined on a empty flat surface [2]. In particular, our implementation considers a $N \times M$ grid and let $p_t(i,j)$ be the number of grains at site (i,j) for each unit time $t \in \mathbb{N}^0$. Assume the surface is empty for now, then adding a grain of sand is defined as:

$$p_t(i,j) = p_t(i,j) + 1.$$

If grains on a single site exceed the critical value, p_c, then a topple is defined as distribute sands to neighboring sites. In particular, if $p_c = 4$, then for any site $p_t(i,j) \geq 4$, the topping rule can be defined as

$$\begin{aligned} p_t(i,j) &= p_t(i,j) - 4, \\ p_t(i \pm 1, j) &= p_t(i \pm 1, j) + 1, \\ p_t(i, j \pm 1) &= p_t(i, j \pm 1) + 1. \end{aligned} \tag{1}$$

Our implementation further assume an open boundary condition is placed, so that grains may fall of the edge. Hence, it is expected the system drives toward a steady state where grains added equal to the grains falling off the edge. Here, one should not confuse a steady state with an equilibrium: an equilibrium often describes a closed system with no driving force, whereas a steady state is associated with open systems, where net change over time is zero. This led us to believe that the system drives toward a stationary state where observables are independent of time, as suggested in previous studies [11]. Illustration of (1) in a single avalanching event can be found in figure 1. An avalanche can be defined as recurrent operations of (1) until $p_t(i,j) \leq 4$, $\forall\, i \in \{1, \cdots, N\}, j \in \{1, \cdots, M\}$. In this case, one can say that a height configuration at any stationary states is a recursion of its previous stationary state. At stationary state, or in a more general context, steady state, avalanche stops and the model will exhibit power-law behavior in metrics like cluster size and duration, as discussed in [1, 2].

We believe that, at steady state, energy inflow (adding grains) and outflow (grains falling off boundary) should be equal. Therefore, the average height of the grid, defined by

$$\langle p_t \rangle := \frac{1}{NM} \sum_{i,j} p_t(i,j), \tag{2}$$

is approximately 2.

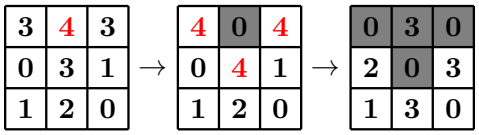

Figure 1: Single avalanche of the model under Abelian toppling rules on a 3×3 grid. The avalanche has a size of 4 and duration of 2.

To further study the avalanche, we will be focusing on the following properties:

Size (s): the number of topples required for the system to relax.

Area (s_d): distinct sites toppled

Loss (l): the number of grains fell off the grid.

Length (ℓ): maximal L^1 distance from the first toppled site

As stated in the original paper [1, 2], frequency distribution of avalanche size s in log-log scale should follow:

$$D(s) \approx s^{-\tau}, \quad \tau \approx 1. \tag{3}$$

We argue that the avalanche area, which is equivalent to the number of distinct topples, s_d, should also follow (3). Unlike avalanche size and area, which are both observables directly from the system, avalanche loss and length are measures primarily for describing the state of particles (grains), we therefore expect them not to follow (3). Instead, to measure all four properties using a single functional form, let

$$D(\mathbf{x}) \approx a\mathbf{x}^{-k},$$

be defined as the frequency distribution of $\mathbf{x} \in \{s, s_d, l, \ell\}$. We intentionally let the length be defined as the L^1 distance as the topple dynamics shown in figure 1 has no diagonal movement. Further discussion on this argument and correlation between these properties will be covered in later sections. Intuitively, avalanche loss is closely related to energy loss in many cases and were used interchangeably by many. In general, a sandpile model that allows energy loss is called a dissipative sandpile model. We believe that the dissipative sandpile model is ergodic, that is, ensemble average is equal to the time average, given the time independent nature of this model [12].

2.2.2 Abelian property

One of the aspect that distinguish Abelian models with other SOC models is the Abelian property. That is, it allows commutative unstable configuration: if there are more than one unstable sites, then one toppling will commute with others (i.e. order does not matter). To show this, let $\Delta(\mathbf{x}, \mathbf{y})$ be the toppling matrix, satisfying the following conditions

$$\forall\, \mathbf{x} \neq \mathbf{y} \in L, \quad \Delta(\mathbf{x}, \mathbf{y}) = \Delta(\mathbf{y}, \mathbf{x}) \geq 0, \tag{4a}$$

$$\forall\, \mathbf{x} \in L, \quad \Delta(\mathbf{x}, \mathbf{x}) < 0, \tag{4b}$$

$$\forall\, \mathbf{x} \in L, \quad \sum_{\mathbf{y} \in L} \Delta(\mathbf{x}, \mathbf{y}) \leq 0, \tag{4c}$$

$$\sum_{\mathbf{x}, \mathbf{y} \in L} \Delta(\mathbf{x}, \mathbf{y}) < 0. \tag{4d}$$

(4a) simply implies the commutativity of unstable configurations. This is indeed important, otherwise one need to keep track of all unstable sites for every single avalanches since toppling of a unstable site may cause other unstable sites to return to stable under non-commutative configurations. Together with (4b), this ensures that only toppled sites lose grains but not other

sites $\mathbf{x} \neq \mathbf{y}$, which is important as one need to make sure there is no energy created inside each toppling processes. (4c) and (4d) combined simply shows that grains may fall of the edge, as stated in the open boundary requirement. In fact, some have argued that a steady state is not possible for a closed one [13]. Now, if (4) are satisfied, then the toppling rule can be defined by

$$\Delta(\mathbf{x}, \mathbf{y}) = \begin{cases} -2d & \mathbf{x} = \mathbf{y} \\ 1 & \mathbf{x}, \mathbf{y} \text{ are nearest neighbors} \\ 0 & \text{otherwise} \end{cases}, \tag{5}$$

where d denotes the dimension. Clearly, in 2D models (i.e. $d = 2$), (5) implies that $\Delta(\mathbf{x}, \mathbf{x}) = -4 = -p_c$, which is the same as the critical height for a site to topple as discussed in 2.2.1. If we put

$$p(\mathbf{x}) = p(\mathbf{x}) + \Delta(\mathbf{x}, \mathbf{x}), \tag{6}$$

where $p(\mathbf{x})$ denotes the height configuration at site $\mathbf{x}$. Then it is the same as previously defined toppling rules in (1), where (4a) and (4b) are clearly satisfied. With (5), we may show that (6) can be generalized to

$$(T_{\mathbf{x}} p)(\mathbf{y}) := \begin{cases} p(\mathbf{y}) + \Delta(\mathbf{x}, \mathbf{y}) & p(\mathbf{x}) \geq \Delta(\mathbf{x}, \mathbf{x}) \\ p(\mathbf{y}) & \text{otherwise} \end{cases}, \tag{7}$$

where $T_{\mathbf{x}}$ is the toppling operator associated with adding a grain at site $\mathbf{x}$. To satisfy commutativity as discussed earlier, we want to show that

$$(T_{\mathbf{x}} \circ T'_{\mathbf{x}})(p) = (T'_{\mathbf{x}} \circ T_{\mathbf{x}})(p). \tag{8}$$

Write the LHS by directly applying (7):

$$(T_{\mathbf{x}} \circ T'_{\mathbf{x}})(p) = \begin{cases} p(\mathbf{y}) + \Delta(\mathbf{x}, \mathbf{y}) + \Delta(\mathbf{x}', \mathbf{y}) & p(\mathbf{x}) \geq \Delta(\mathbf{x}, \mathbf{x}) \text{ and } p'(\mathbf{x}') \geq \Delta(\mathbf{x}', \mathbf{x}') \\ p(\mathbf{y}) + \Delta(\mathbf{x}, \mathbf{y}) & p(\mathbf{x}) \geq \Delta(\mathbf{x}, \mathbf{x}) \text{ only} \\ p(\mathbf{y}) + \Delta(\mathbf{x}', \mathbf{y}) & p'(\mathbf{x}) \geq \Delta(\mathbf{x}', \mathbf{x}') \text{ only} \\ p(\mathbf{y}) & \text{otherwise} \end{cases}$$

Observe that RHS of (8) is the same as the above given the same configuration $p(\mathbf{y})$, with the only difference in the toppling order $p(\mathbf{y}) + \Delta(\mathbf{x}', \mathbf{y}) + \Delta(\mathbf{x}, \mathbf{y})$. According to the toppling rule defined in (5), it is obvious that (8) hold.

In general, (8) can describe an avalanche, by introducing the stabilization operator,

$$\mathbb{T} : U_L \to S_L,$$

where U_L is the space of all possible height configurations and $S_L \subset U_L$ is the space of stable height configurations; such an operator can be defined by

$$\mathbb{T} = \prod_{i=1}^{N} T_{\mathbf{x}_i} \tag{9}$$

To show that (9) is well-defined, consider two sequences of vertices

$$\mathbf{x}_1, \mathbf{x}_2, \cdots, \mathbf{x}_n,$$
$$\mathbf{y}_1, \mathbf{y}_2, \cdots, \mathbf{y}_m,$$

that both form stabilizing sequences of p, describing series of (possible) toppling events. If p is stable, then $n = m = 0$; if p is unstable, then $\mathbf{x}_j$ must be somewhere in the $\mathbf{y}_1, \mathbf{y}_2, \cdots, \mathbf{y}_m$

sequence according to (8). Without loss of generality, assume that $j = 1$, so that $\mathbf{x}_1 = \mathbf{y}_i$, for some $1 \leq i \leq m$. Further assume that i is the smallest index, then by (8), it follows that

$$\begin{aligned}(T_{\mathbf{x}_1} T_{\mathbf{y}_{i-1}} \cdots T_{\mathbf{y}_1})(p) &= (T_{\mathbf{y}_{i-1}} T_{\mathbf{x}_1} T_{\mathbf{y}_{i-2}} \cdots T_{\mathbf{y}_1})(p) \\ &\vdots \\ &= (T_{\mathbf{y}_{i-1}} \cdots T_{\mathbf{y}_1} T_{\mathbf{x}_1})(p),\end{aligned}$$

which suffices to show that the sequence

$$\mathbf{x}_1, \mathbf{y}_1, \cdots, \mathbf{y}_{i-1}, \mathbf{y}_{i+1} \cdots \mathbf{y}_m$$

is also a stabilizing sequence of p. Therefore for any configuration p, the stabilizing operator $\mathbb{T}p = p'$ is unique, and thus well defined.

2.3 Extend the sandpile model

2.3.1 Stochastic sandpile model

In general, stochastic sandpile models are variants which exhibit stochastic behavior, or in simple terms, randomness. Although there has been dispute on the exact definition, it was believed that the manna model was the first implementation [5]. Later studies have shown some Abelian properties of this model [14, 15], yet disagreed by others [7]. Our implementation is defined on the same basis as discussed in 2.2.2 with a stochastic toppling rules. That is, whenever $p_t(i, j) \geq 4$, it follows that

$$p_t(i, j) = p_t(i, j) - 4$$

where 4 of the neighboring sites of (i, j) are randomly selected form 8 neighbors $(i \pm 1, j \pm 1)$ with certain probability. Immediately, one may recognize that this model satisfy eq. (4), which certainly pertains some Abelian properties. Although later results and [11, 16] suggested that this variant does resemble the Abelian model in many ways, and even showing some Abelianity, it is often studied under other universality class. We will not go through these arguments here but focus on the same properties that characterize a sandpile model. Moreover, we are also interested in $\{s, s_d, l, \ell\}$ of this model and observing them in the power-law spectrum.

Recurrent topple in this model follows the same principle as Abelian model does, except for each toppling at $p(\mathbf{x})$, its neighbors, $\mathbf{y}$, are randomly selected. The probability of each neighboring sites being chose is assumed to be the same in later simulation as our focus is to compare across models but not study an individual one.

2.3.2 Non-Abelian sandpile model

By definition, non-Abelian groups fail to satisfy commutativity. Therefore, models that fail to satisfy (4a) can be classified as a non-Abelian sandpile model. We have already shown the importance of commutativity, and argued that it is impossible to record an avalanche if there are multiple stabilizing configurations.

In particular, our implementation is similar to the directed slope and critical slope method [8, 17], where we consider slopes measured from neighboring sites. Let p_c be local height threshold, if any of the four instability conditions:

$$\begin{aligned}p_t(i, j) - p_t(i + 1, j) &\geq p_c, \\ p_t(i, j) - p_t(i - 1, j) &\geq p_c, \\ p_t(i, j) - p_t(i, j + 1) &\geq p_c, \\ p_t(i, j) - p_t(i, j - 1) &\geq p_c,\end{aligned} \tag{10}$$

is satisfied, then the site will topple, defined by

$$\begin{aligned} p_t(i,j) &= p_t(i,j) - p_c, \\ p_t(i \pm 1, j) &= p_t(i \pm 1, j) + 1, \\ p_t(i, j \pm 1) &= p_t(i, j \pm 1) + 1. \end{aligned} \tag{11}$$

Initially, (11) seems to follow a similar toppling scheme as (1). However, given the instability condition, one should notice that steady state can also be achieved by adding grains of sand. Suppose there are initially two unstable sites, relatively close to each other so that some neighbors are shared. Clearly, if one site toppled and grains are distributed to neighboring sites, the other unstable may become stable without toppling as one of the instability conditions may break. Illustration of non-Abelian topple rule can be found in figure 2, where we can see two non-commutative stabilizing sequences are exclusive to each other.

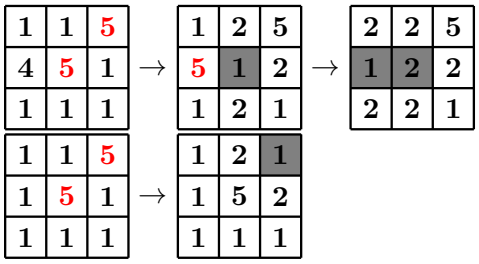

Figure 2: Single avalanche of the critical slope model on a 3×3 grid. Two unstable configurations cause non-commutative stabilizing sequences with different avalanching statistics

We notice that this model is in its nature less stable than other variants as introduction of a single sand can effect multiple sites. To be more specific, adding a grain of sand can change local gradients of all adjacent site. If there more gradient measures are taken near a single site, then it will be more likely for it to satisfy any of the instability conditions, thus leading to an avalanche. Therefore, we think this gradient-based model is a more realistic model in simulating the sand slide dynamics. Implementing a model that consider all possible stabilizing sequences can be hard, or even impossible once the grid gets sufficiently large. Here we introduce a stochastic implementation similar to the stochastic toppling rules shown in 2.3.1. In particular, the model can be simplified into following procedures:

i. Look for sites that satisfy any of (10), record these sites with different sequences based on which slope measure is taking.

ii. Choose one from all available sequences randomly, and topple them. Because no adjacent sites can be both unstable under the same slope measure, stabilizing one does not break the instability of other.

iii. Repeat i. and ii. until no sites are unstable.

Note that (11) can be generalized by changing the slope measures in (10). For example, some have proposed a variant with only $p_t(i,j) - p_t(i,j+1)$ and $p_t(i,j) - p_t(i+1,j+1)$ are measured [17]. We may think of slope measure as the surface is directed toward that specific direction, which gives sandpiles from the above model a pyramid-like shape [8]. We argue that the threshold for instability p_c must be greater than or equal to the number of slope measures. Otherwise, a hole will form and the avalanche never stops and the unstable sites keep distributing grains even when they reach negative height. This is be visualized as hole-digging process [8]; yet, as the avalanche does not terminate and the model will never reach a steady state, no useful statistics can be collected.

2.4 Implementation method

2.4.1 General development

Every model discussed earlier will be placed on a $N \times M$ grid, initially empty or randomly filled with grains and set to relax. In particular, three types of grain drops will be considered: drop at a random site, a specific site and randomly drop around a specific site that follows Gaussian distribution.

Recall that all models are placed in a open system. A "standard" approach to solve boundary conditions involves multiple branching (conditional) statements, which requires heavy computation forces for each avalanche once the simulation grid gets sufficiently large. Hence, we introduce a simulation boundary (padding) that surrounds the grid, so that grains fell on the simulation boundary are counted as lost. Meanwhile, the value from each site on this boundary is reset to zero after a single avalanche is terminated, so that it would not introduce any new unstable sites. We note that this boundary is not only helpful when collecting energy loss, but also allows more complex dynamics by adjusting the size of boundary.

To collect $\{s, s_d, l, \ell\}$, one can simply search for unstable sites and compute their sizes to get s. We use a mask matrix *area* with the same size as the sandpile grid to record s_d: if a site (i, j) is toppled then $area[i, j] = \texttt{True}$. And l is calculated as the sum of grains on the simulation boundary as argued above. To collect ℓ, we must first find a possible "origin", which can be one or mores unstable sites. ℓ is defined as the reach of an avalanche, and is calculated by the maximum Manhattan distance within a single avalanche. Finally, because the power-law distribution is interpreted as a straight line in logarithmic scale, it is convenient to linearly fit data in log space. However, due to the heavy-tailedness, we decided to fit with certain percentiles of data, where the exact percentile is determined by the the heavy-tailedness of the data (for example 1-90th percentile for s, s_d and 1-70th percentile for l, ℓ).

Although the toppling rules differ and the development is highly subjected to models, we propose a general structure of this model as shown in figure 3. In particular, we use a while loop to search for and topple unstable sites, whose process is shown by the following pseudocode:

Search for unstable sites $p[i, j]$
Initialize metrics for collecting statistics
while $p[i, j]$ unstable **do**
    $p[i, j] \leftarrow p[i, j] - p_c$ ▷ p_c is the threshold for stability
    $p[i \pm 1, j \pm 1] \leftarrow p[i \pm 1, j \pm 1] + 1$
    Update statistics
    Search for unstable sites $p[i, j]$

Here, $p[i, j]$ can be more than one site; we rely on the `numpy` library from Python to find all possible unstable sites and topple them all at once. Compared with a draft version implemented with serial searching and toppling, this parallel version runs significantly faster, as suggested in [18].

2.4.2 Model specific development

Intuitively, implementations of Abelian and stochastic models are straightforward based on the toppling rule defined in (5). The non-Abelian model, on the other hand, is more subtle to compute as most of the existing library only supports row or column-wise gradient computation. To further generalize this model so that gradients can be take from any direction, we use the

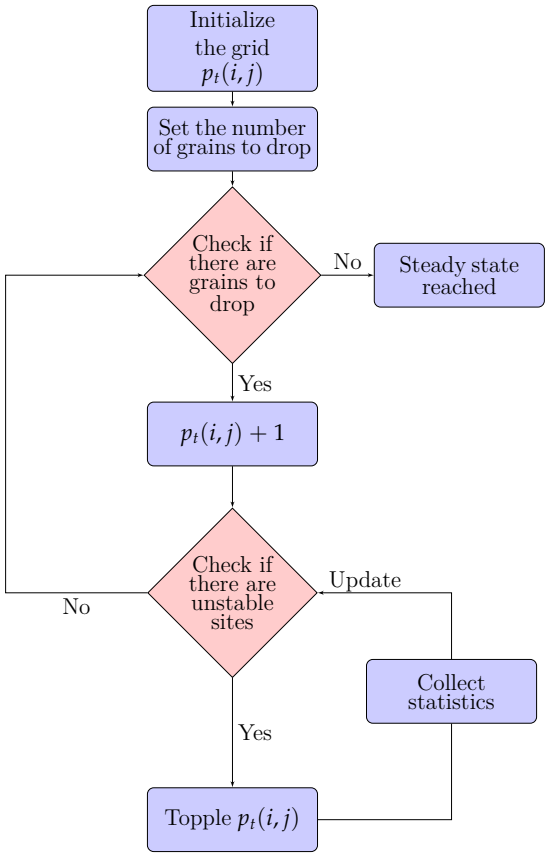

Figure 3: Flow chart illustration of the key architecture for sandpile models

convolution window, a technique often used in image processing to enhance local pixels. The general form for matrix convolution is

$$\begin{bmatrix} x_{11} & x_{12} & \cdots & x_{1n} \\ x_{21} & x_{22} & \cdots & x_{2n} \\ \vdots & \vdots & \ddots & \vdots \\ x_{m1} & x_{m2} & \cdots & x_{mn} \end{bmatrix} * \begin{bmatrix} y_{11} & y_{12} & \cdots & y_{1n} \\ y_{21} & y_{22} & \cdots & y_{2n} \\ \vdots & \vdots & \ddots & \vdots \\ y_{m1} & y_{m2} & \cdots & y_{mn} \end{bmatrix} = \sum_{i=0}^{m-1} \sum_{j=0}^{n-1} x_{(m-i)(n-j)} \cdot y_{(1+i)(1+j)}. \tag{12}$$

Note that matrices do not have to be of the same size; rather, $\sum_{i=1}^{m} \sum_{j=1}^{n} x_{ij}$ can be seen as a sub-matrix from a bigger matrix (for example $\sum_{i=1}^{m+r} \sum_{j=1}^{n+r} x_{ij}$), so that the convolution is interpreted as the local feature of such matrix, filtered by $\sum_{i=1}^{m} \sum_{j=1}^{n} y_{ij}$. Hence, to have the entire matrix filtered, one can "shift" the kernel to the right by k ($k \leq r$) steps, where (12) becomes

$$\begin{bmatrix} x_{1(1+k)} & x_{1(2+k)} & \cdots & x_{1(n+k)} \\ x_{2(1+k)} & x_{2(2+k)} & \cdots & x_{2(n+k)} \\ \vdots & \vdots & \ddots & \vdots \\ x_{m(1+k)} & x_{m(2+k)} & \cdots & x_{m(n+k)} \end{bmatrix} * \begin{bmatrix} y_{11} & y_{12} & \cdots & y_{1n} \\ y_{21} & y_{22} & \cdots & y_{2n} \\ \vdots & \vdots & \ddots & \vdots \\ y_{m1} & y_{m2} & \cdots & y_{mn} \end{bmatrix} = \sum_{i=0}^{m-1} \sum_{j=0}^{n-1} x_{(m-i)(n+k-j)} \cdot y_{(1+i)(1+j)}.$$

Similarly, for downward shifts, the row index is shifted by k (i.e. $m+k$). As shown in figure 4a, to calculate the gradient $p(i,j) - p(i+1, j+1)$, apply kernel $\left[\begin{smallmatrix} -1 & 0 \\ 0 & 1 \end{smallmatrix}\right]$ to get

$$(1 \times -1) + (2 \times 0) + (3 \times 0) + (1 \times 1) = 0.$$

If we follow the same principle and shift the kernel right or down by one as shown in 4b until it traverses the entire matrix, then the resulting output is $\left[\begin{smallmatrix} 0 & 0 \\ -1 & 1 \end{smallmatrix}\right]$, exactly equals to the gradient we

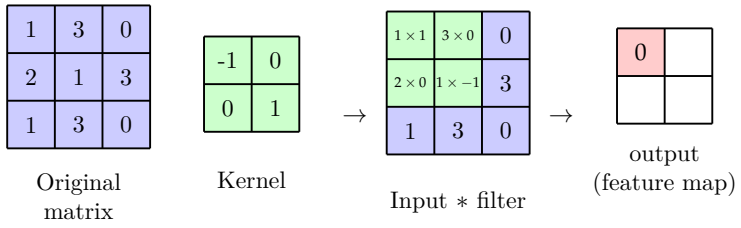

(a) Illustration of local matrix convolution

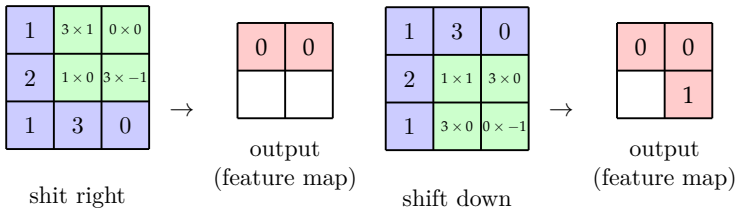

(b) Illustration of kernel shifting

Figure 4: Convolution of a 3×3 matrix using 2×2 kernel under "valid" shift; result interpreted as gradient of adjacent diagonal entries

require. To measure gradients from other direction, one can simply change the kernel based on (12). For example, to compute the gradient $p(i,j) - p(i,j+1)$, one may use the kernel $\left[\begin{smallmatrix} 0 & -1 \\ 0 & 1 \end{smallmatrix}\right]$. Note that this technique can be applied to further generalize the non-Abelian model; for example, if we want instability condition based on relative gradient taken from two entries along the same direction, increase the kernel size by 1 and change its entries accordingly would suffice.

3 Computational Results

We will begin this section by showing some generic results in proving previous hypothesis and justification. We argued that the average height of sandpile models should be approximately 2, which is true as shown in figure 5, similar to a proven result, 17/8, in [19].

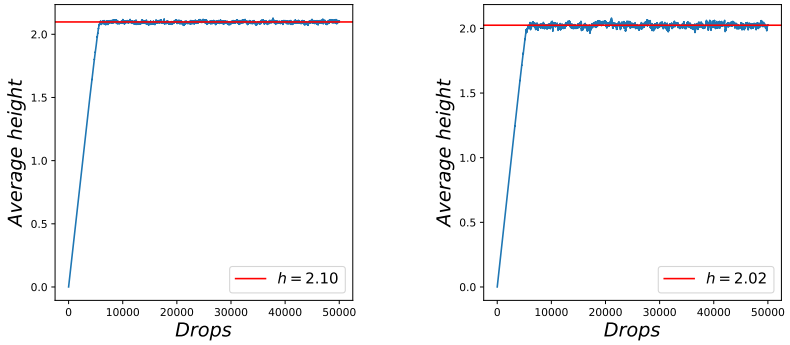

(a) Abelian sandpile model (b) stochastic sandpile model

Figure 5: Average height of sandpile models over 5×10^4 drops on 50×50 grid

We have also argued that L^1 norm is a better description of avalanche lengths based on the specific dynamics of our models. This is indeed true if we look at the results shown in figure 6. Although both figures suggest good power-law fits, there are more noises in L^2 distance, due to the squared error.

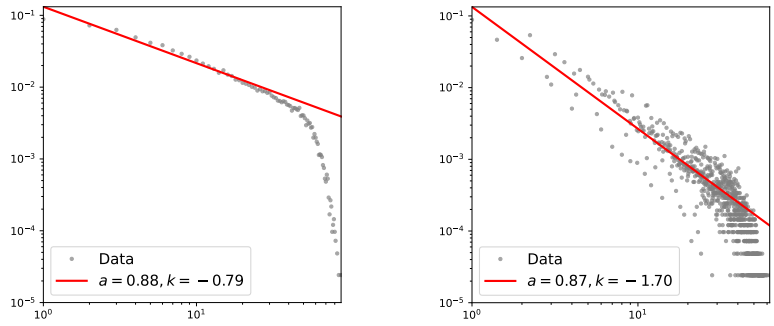

(a) L^1 (b) L^2

Figure 6: Avalanche lengths as (a) L^1 norm and (b) L^2 norm

3.1 Abelian sandpile model

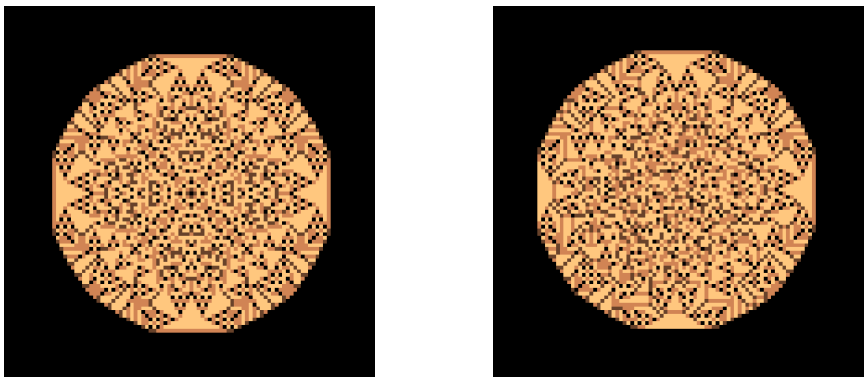

(a) 10^4 grains continuously dropped at the center (b) 10^4 grains normally distributed near ($\sigma^2 = 5$) the center

Figure 7: Scale-invariant patterns displayed in limiting shape of the Abelian sandpile model on a 100×100 grid

Figure 8 in general displays a relatively convincing power-law behavior, as indicated by the critical exponent marked in red; finite size cutoff is also observed, as suggested by previous studies [2, 6, 8]. The figure also verifies our previous assumptions that critical exponents characterising avalanche loss, l, and length, ℓ, does not equal ones from s and s_d. They are in nature associated with particle dissipation and travel distance, respectively. In particular, we observe that figure 8a and 8c share a similar critical exponent result, $k \approx 1$, for both s and s_d, a good agreement with [2]. Profiles in figure 8b all show humps near the cutoff, which is further confirmed by 8c. Use figure 7 , we argue that continuous drops at a specific site is the same as a normal distribution of drops near that site, which yields the same dynamics that translates to a slightly organized avalanche pattern (fractal-like, as shown in figure 7), where the heavy-tailedness is amplified, exhibiting a hump-like shape. We call this a "centralized" effect, where most avalanche data are clustered to some specific values due a centralized inflow of energy near one point in the spatial domain, as indicated in plots of s_d.

In general, the system clearly drives itself to criticality as indicated by the above statistics. And the introduction of stochasticity in grain addition does yield a more convincing power-law fit in all four profiles. In particular, we made drops in the figure 8a completely random so that it return a tighter fit to the power-law function than Gaussian drop does.

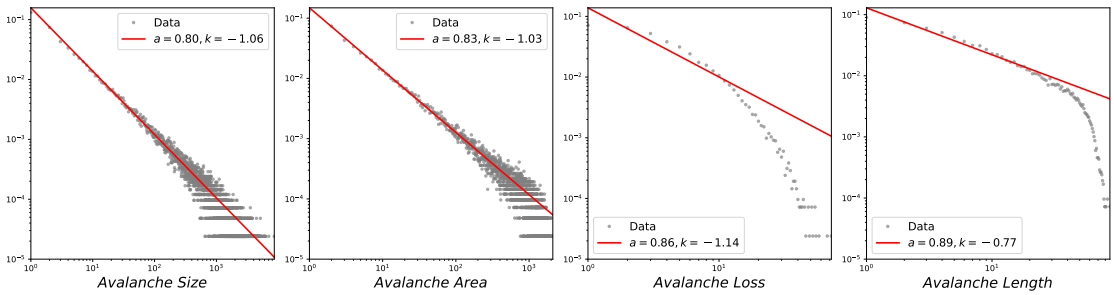

(a) Random drops

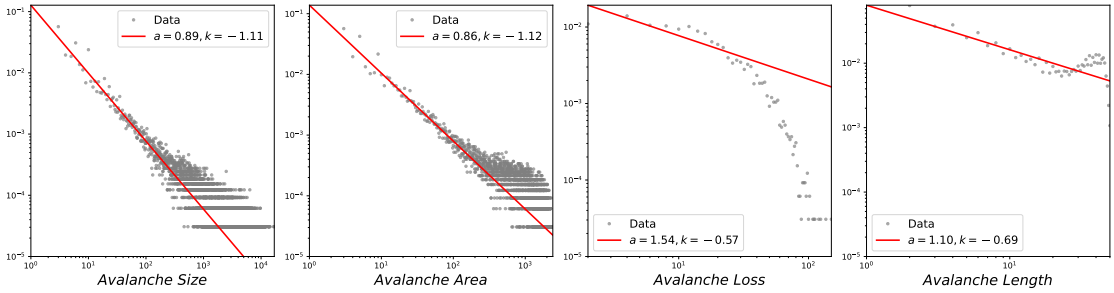

(b) Continuous drops at the center of the grid

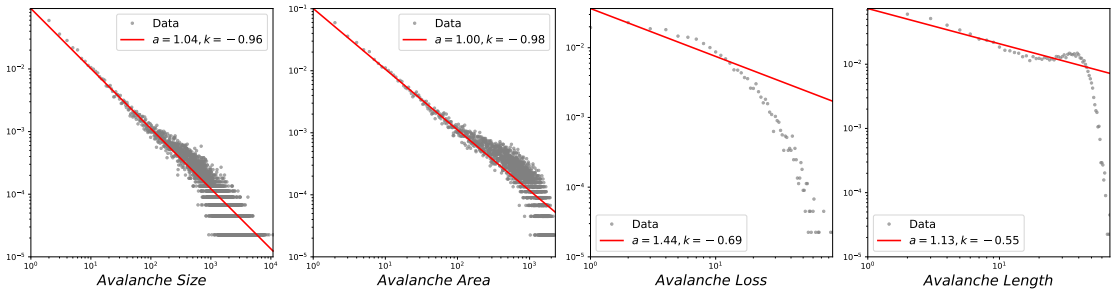

(c) Normally distributed near the center of the grid ($\mathcal{N}\{(25,25),5\}$)

Figure 8: Frequency distribution of statistics in double logarithmic scale; collected from Abelian sandpile model with 10^5 grains dropped on a 50×50 grid; distribution plots ordered from first to last column: $\{s, s_d, l, \ell\}$

Despite of the interesting power-law behavior displayed in the distribution of $\{s, s_d, l, \ell\}$ and scale-inavriance pattern shown in its limiting shape, dynamics shown in this model is clearly unrealistic.

3.2 Stochastic sandpile model

In general, distribution of s and s_d collected from the stochastic variant share a similar critical exponent result, $k \approx 1.2$, under all dropping configurations. With its resemblance to 4-state Potts model in terms of critical exponent of the driving force response [7, 11], we believe that this model belongs to the Ashkin-Teller criticality class.

By comparing figure 8 and 9, we observe that distributions plots for each of $\{s, s_d, l, \ell\}$ under same dropping configuration are very similar between these models. Moreover, figure 9b and 9c further confirm that dropping near (or at) a specific site does introduce a hump-like shape near the cutoff, due to the centralized effect.

A careful inspection on figure 9 convinced us that this stochastic variant is less sensitive to dropping configuration, unlike what we have shown in the Abelian model. We believe that the randomness in toppling makes this model less dependent on local dynamics.

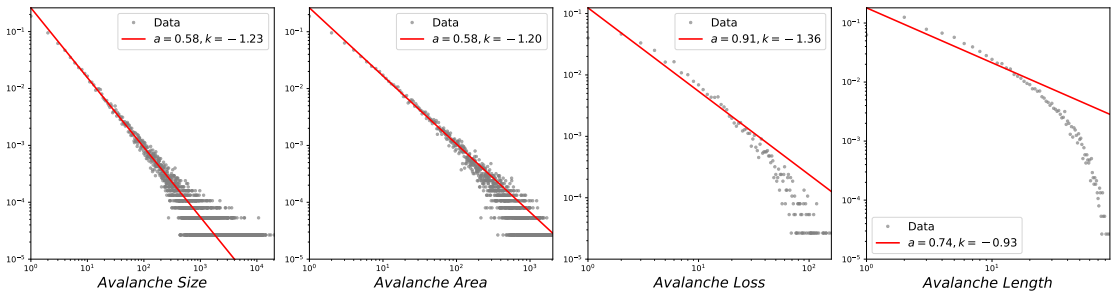

(a) Random drops

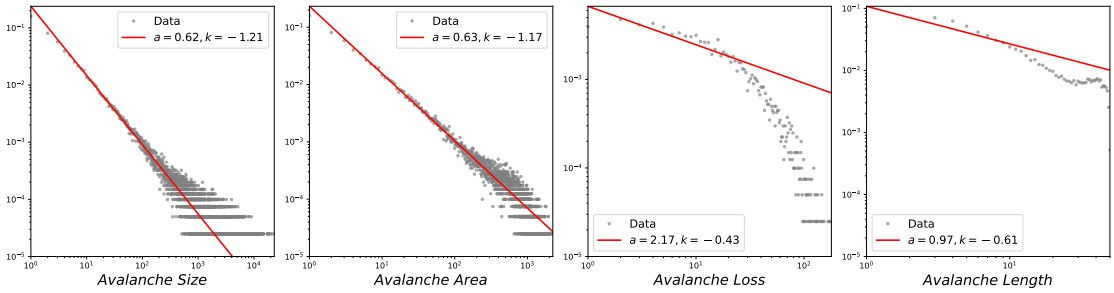

(b) Continuous drops at the center of the grid

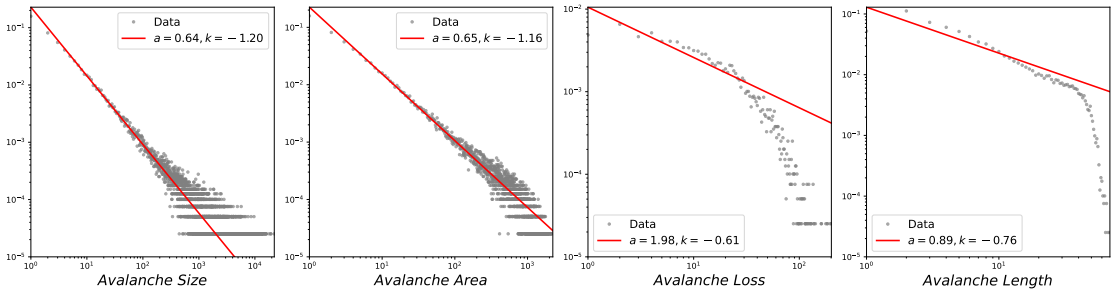

(c) Normally distributed near the center of the grid ($\mathcal{N}\{(25,25),5\}$)

Figure 9: Frequency distribution of statistics in double logarithmic scale; collected from stochastic sandpile model with 10^5 grains dropped on a 50×50 grid; distribution plots ordered from first to last column: $\{s, s_d, l, \ell\}$

3.3 Non-Abelian sandpile model

In earlier sections, we discussed the motivation of this model. That is, a directed slope model whose instability is introduced by local gradient, as shown in figure 10. In particular, figure 10a represents the dynamics of a sand slide on a sloped surface whereas figure 10b shows the sand pile forms a pyramid. We observe that grains near the boundary are of less height because they may fall off and less likely to accumulate, corresponding to the fact that grains on the boundary of a sloped surface tend to get pushed off by other as suggested by many practical experiments.

This model also presents a more realistic avalanching dynamics shown in figure 11. By comparing figure 11a, 11b and 11c, we observe that all sand dropping scheme drive to similar limiting-shapes, which resembles sand drops in reality as shown figure 12. For avalanching statistics shown in figure 13, only 13a agrees with previous results. We found that distribution for s and s_d in figure 13a are particularly similar to ones in figure 8a. In fact, they both share a critical exponent $k \approx 1$, unlike what some studies have suggested [8, 17]. We believe that this discrepancy is caused by a combination of finite size scaling effect and implementation method.

Uncharacteristic behaviors are observed in both figure 13b and 13c. The amount of outliers in distribution plots of avalanche size and area suggest remarkable heavy-tailedness. In 3.1, we

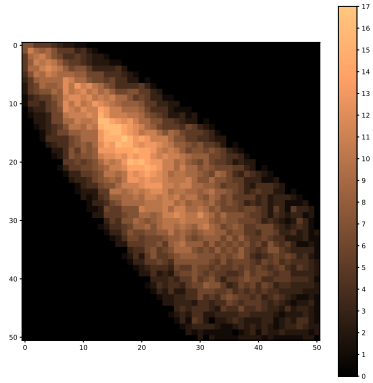

(a) Slopes measured from $p_t(i, j+1)$ and $p_t(i+1, j+1)$; 10^4 drops at $(0, 0)$

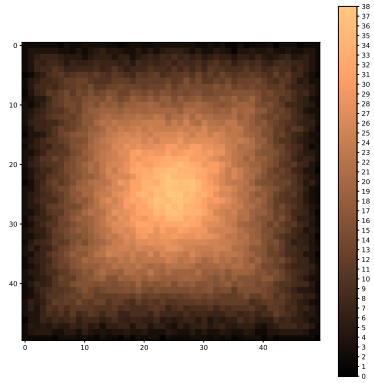

(b) Slopes measured from $p_t(i \pm 1, j)$ and $p_t(i, j \pm 1)$; 10^5 drops at $(25, 25)$

Figure 10: Limiting shapes of non-Abelian sandpile model on a 50×50 grid with different gradient measures

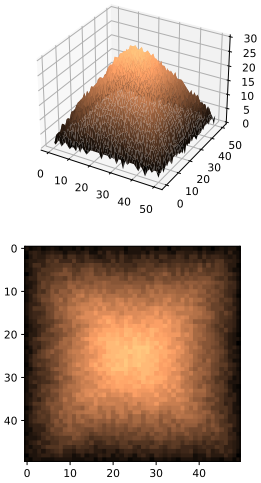

(a) Random drops

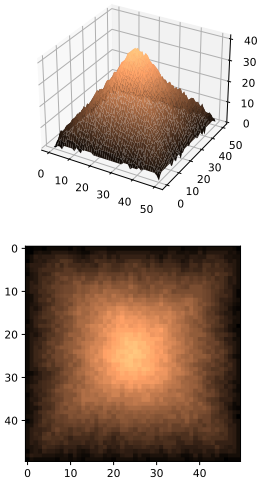

(b) centered drops

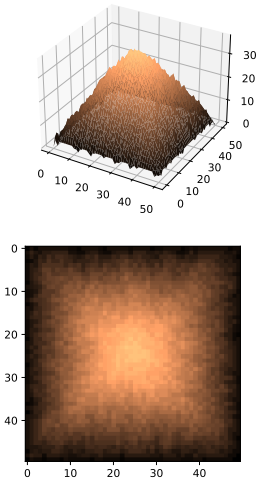

(c) Gaussian drops

Figure 11: Limiting shapes of non-Abelian sandpile model on a 50×50 grid after 5×10^4 drops; slopes measured from four cardinal neighbors as in (10);

Figure 12: Example of sandpile shapes formed in real life by continuous drops [20]

have shown that dropping near a specific site increases heavy-tailedness, thus generates humps in distribution plots, which holds for this model as well, where the hump is translated to even larger avalanches. As discussed earlier, a sandpile model defined with gradient-based toppling rule is in its nature less stable than the other variants since the addition of a single grain of sand could change local gradient significantly. Coupled with the centralized effect of sand drops, later recursions find significantly large avalanches ($s > 10^5$), indicating a collapse of sand from

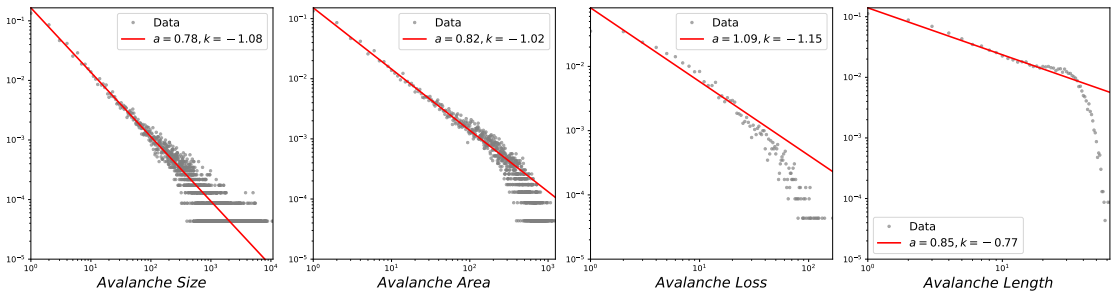

(a) Random drops

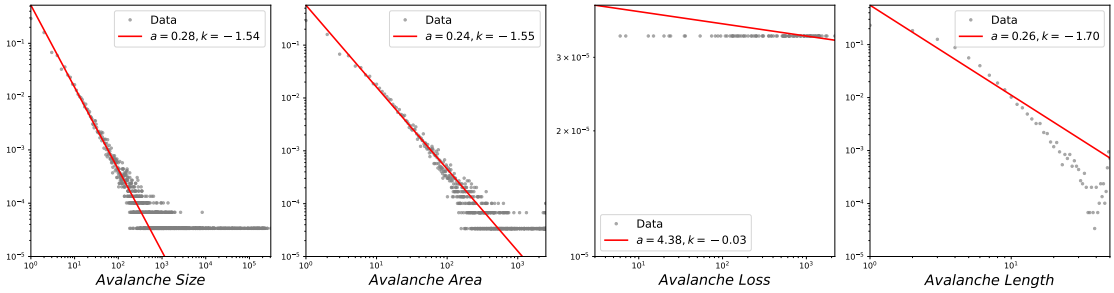

(b) Continuous drops at the center of the grid

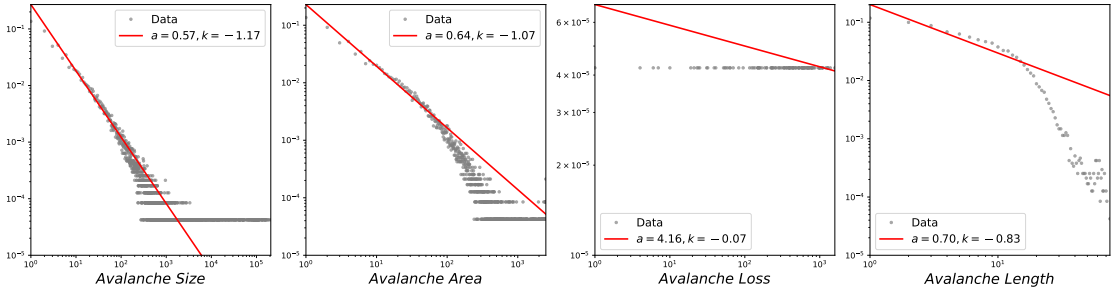

(c) Normally distributed near the center of the grid ($\mathcal{N}\{(25,25),5\}$)

Figure 13: Frequency distribution of statisitics in double logarithmic scale; collected from non-Abelian sandpile model with 10^5 grains dropped on a 50×50 grid; distribution plots ordered from first to last column: $\{s, s_d, l, \ell\}$

the center. For avalanche loss distributions, we observe that a great amount of sand grains were lost throughout the relaxation, which is indeed true considering abnormal avalanche sizes.

3.4 Model runtime

Another thing to note in this section is the overall runtime. Although the exact complexity cannot be studied due to the self-driven nature of this model, results collected from 20 sample runs on a Intel i7-9700 CPU with random drops between 5×10^4 and 10^5 on the Abelian model suggest a linear growth rate in runtime. However, a quadratic growth rate is recorded when comparing results form runs with random drops between 10^5 and 10^6. Based on theses test cases, we reaffirm that the sandpile model in 2D is indeed P-complete and its complexity remains unassertive [18].

For sand-dropping configuration-wise comparison, the Abelian and stochastic models both admit a random drops $>$ gaussian drops $\geq$ centered drops rank in terms of runtime. On the other hand, the non-Abelian model runs slightly faster on the random drop configuration compared to centered drops and Gaussian drops. We believe that this is also due to the extended heavy-tailedness of centralized effect since in general larger s and s_d translates to longer avalanche

duration. As the non-Abelian toppling rule is more unstable and does not admit any predefined patterns like the Abelian ones, longer avalanche duration does imply longer runtime.

As for model-wise runtime comparisons, we sampled 10 runs from each of these models and record a ranking of Abelian $\leq$ stochastic $<$ non-Abelian in general. One should not be surprised about this result as the Abelian sandpile model is particularly well defined under various metrics. The stochastic version reports an average runtime 87.6 s, slightly slower than 84.3 s for the Abelian model on a 50×50 grid over 5×10^4 grains of sand.

4 Conclusion and Discussion

In this report, we studied the sandpile model and its characteristics by carefully examining related works and simulation results. Despite showing scale-invaraiance patterns in its limiting shape, the dynamics from the Abelian models is no where close to a real sandpile dynamics. We showed that non-Abelian sandpile does produce a better simulation to the real-world dynamics of sandpiles by identifying its limiting shapes in 3D, where we set a new scheme for implement this type of models via convolution window and simulation boundary.

s, s_d	Model		
Dropping configuration	Abelian	Stochastic	non-Abelian
Random drops	1.01 ± 0.05	1.21 ± 0.05	1.05 ± 0.05
Centered drops	1.11 ± 0.01	1.19 ± 0.02	1.55 ± 0.03
Gaussian drops	0.99 ± 0.03	1.18 ± 0.02	1.15 ± 0.03

Table 1: Critical exponent result for s, s_d on average across different models

l	Model		
Dropping configuration	Abelian	Stochastic	non-Abelian
Random drops	1.14 ± 0.02	1.34 ± 0.02	1.17 ± 0.03
Centered drops	0.57 ± 0.01	0.44 ± 0.01	N/A
Gaussian drops	0.68 ± 0.03	0.61 ± 0.02	N/A

Table 2: Critical exponent result for l across different models

ℓ	Model		
Dropping configuration	Abelian	Stochastic	non-Abelian
Random drops	0.91 ± 0.3	0.93 ± 0.04	1.17 ± 0.03
Centered drops	0.61 ± 0.01	0.60 ± 0.02	1.71 ± 0.02
Gaussian drops	0.73 ± 0.03	0.75 ± 0.03	0.85 ± 0.03

Table 3: Critical exponent result for ℓ across different models

The overall power-law behavior for all models are ensured, but strong disagreement in critical exponents collected across different models, as shown in table 1, suggest that they are belong to different problem classes. In general, $k \approx 1$ for $\{s, s_d\}$ was reported for both Abelian and non-Abelian model with random drop. We disagree with [7] that non-Abelian model belongs to the Universality class. Instead, matching results convinced us that the stochastic-based non-Abelian model can also be used to explain $1/f$ noise, and thus should be also studied as a SOC system. The stochastic model, on the other hand, resembles the four-state Potts model [11]. We believe

that this model should be studied under Ashkin-Teller criticality as the critical exponent result, $k \approx 1.2$, for driving force responses, $\{s, s_d\}$, fits in this problem class.

For l and ℓ, the mechanism is still uncertain; yet we do agree on the fact that they both obey the power-law distribution and can be used to distinguish different types of model. l in particular, as a indication of energy dissipation, is highly dependent on the dropping configuration as shown in table 2. Coupled with figs. 8, 9 and 13, one may observe that random drops produce better power-law fits. We here prove that random dropping is clearly necessary as implicated in the original paper [2]. As for ℓ, although statistics collected do agree with other studies [17], we have not discovered any correlations with any of the $\{s, s_d, l\}$ nor a physical interpretation of it. Yet, given the distribution plots and overall power-law fitting result, we do believe that it is a characteristic metric for sandpile models.

Upon concluding these results, we find that SOC is a special case of dissipative system that is in favour of stochastic energy inflow (grain addition), whereas a fixed energy system belongs to the directed percolation class [21]. Dissipation occurs as the system interacts with environment by exchanging energy and matter. A system that obeys SOC change its behavior by dissipating energy to the environment, where, in the modeling perspective, the system tune its own parameters after every phase transition. As phase transition becomes more drastic in later evolution, this leads to a power-law distribution of deterministic properties.

References

[1] P. Bak, C. Tang and K. Wiesenfeld, 'Self-organized criticality: an explanation of the 1/f noise', Phys. Rev. Lett. **59**, 381–384 (1987) 10.1103/PhysRevLett.59.381.

[2] P. Bak, C. Tang and K. Wiesenfeld, 'Self-organized criticality', Phys. Rev. A **38**, 364–374 (1988) 10.1103/PhysRevA.38.364.

[3] C. Tang and P. Bak, 'Critical exponents and scaling relations for self-organized critical phenomena', Phys. Rev. Lett. **60**, 2347–2350 (1988) 10.1103/PhysRevLett.60.2347.

[4] H. F. Chau and K. S. Cheng, 'Generalized sandpile model and the characterization of the existence of self-organized criticality', Phys. Rev. A **44**, 6233–6240 (1991) 10.1103/PhysRevA.44.6233.

[5] S. Manna, 'Two-state model of self-organized criticality', Journal of Physics A: Mathematical and General **24**, L363–L369 (1991) 10.1088/0305-4470/24/7/009.

[6] D. Dhar and S. S. Manna, 'Inverse avalanches in the abelian sandpile model', Phys. Rev. E **49**, 2684–2687 (1994) 10.1103/PhysRevE.49.2684.

[7] E. Milshtein, O. Biham and S. Solomon, 'Universality classes in isotropic, abelian, and non-abelian sandpile models', Phys. Rev. E **58**, 303–310 (1998) 10.1103/PhysRevE.58.303.

[8] S. Manna, 'Critical exponents of the sand pile models in two dimensions', Physica A: Statistical Mechanics and its Applications **179**, 249–268 (1991) 10.1016/0378-4371(91)90063-I.

[9] W. Pegden and C. K. Smart, 'Convergence of the abelian sandpile', Duke Mathematical Journal **162**, 627–642 (2013) 10.1215/00127094-2079677.

[10] L. Levine, W. Pegden and C. Smart, 'Apollonian structure in the abelian sandpile', Geometric and Functional Analysis **26**, 306–336 (2012).

[11] D. Dhar, 'The abelian sandpile and related models', Physica A: Statistical Mechanics and its Applications **263**, 4–25 (1999) 10.1016/s0378-4371(98)00493-2.

[12] A. A. Járai, F. Redig and E. Saada, 'Approaching criticality via the zero dissipation limit in the abelian avalanche model', Journal of Statistical Physics **159**, 1369–1407 (2015) 10.1007/s10955-015-1231-z.

[13] D. Dhar, 'Self-organized critical state of sandpile automaton models', Phys. Rev. Lett. **64**, 1613–1616 (1990) 10.1103/PhysRevLett.64.1613.

[14] D. Dhar, 'Some results and a conjecture for manna's stochastic sandpile model', Physica A: Statistical Mechanics and its Applications **270**, 69–81 (1999) 10.1016/s0378-4371(99)00149-1.

[15] J.-F. Marckert, T. Selig and Y.-B. Chan, 'A natural stochastic extension of the sandpile model on a graph', Journal of Combinatorial Theory, Series A **120**, 1913–1928 (2013).

[16] F. Nunzi, 'On the abelianity of the stochastic sandpile model', arxiv (2016), eprint: 1607.05561.

[17] S. S. Manna, 'Sandpile models of self-organized criticality', Current Science **77**, 388–393 (1999).

[18] C. Moore and M. Nilsson, Journal of Statistical Physics **96**, 205–224 (1999) 10.1023/a:1004524500416.

[19] A. A. Járai, 'Sandpile models', Probab. Surveys **15**, 243–306 (2018) 10.1214/14-PS228.

[20] R. Argenton, *Sandpile matemateca 06*, [Online; accessed November, 08, 2020], 2016.

[21] M. Basu et al., 'Fixed-energy sandpiles belong generically to directed percolation', Physical Review Letters **109**, 10.1103/physrevlett.109.015702 (2012) 10.1103/physrevlett.109.015702.